Nuclear Instruments and Methods in Physics Research B 536 (2023) 132–137

Contents lists available at ScienceDirect

Nuclear Inst. and Methods in Physics Research, B

journal homepage: www.elsevier.com/locate/nimb

Surface characterization of CaF_2 crystals irradiated with MeV ions below charge state equilibrium

Rajdeep Kaur *, Petter Ström, Daniel Primetzhofer

Department of Physics and Astronomy, Applied Nuclear Physics, Uppsala University, Uppsala, Sweden

ARTICLE INFO

Keywords:
Ion irradiation
CaF_2
Atomic force microscopy
Nanostructures
Surface modification

ABSTRACT

Single crystals of CaF_2, cleaved along the (1 1 1) plane, were irradiated by ^{35}Cl, ^{39}K, ^{52}Cr, ^{58}Ni, ^{79}Br and ^{197}Au ions with energies from 2 to 48 MeV, charge states from 1+ to 11+ and ion fluences from 2×10^{10} to 1×10^{13} ions/cm^2. The surface properties of the irradiated samples were studied using Atomic Force Microscopy in contact mode. Nanoscale surface structures were observed for some surfaces irradiated by Cl, K, Cr, Ni, Br and Au ions. Thresholds for nanostructure formation were found in terms of projectile ion velocity and electronic stopping power (S_e). Clear surface modification was observed for projectiles with specific energies above approximately 0.04 MeV/u. The threshold in S_e for the generation of distinct triangular structures was observed to be velocity-dependent. The average formation efficiency, referring to the ratio of the number of distinct nanostructures observed on the surface to the number of incident ions, as well as the average height of nanostructures increases with S_e.

1. Introduction

Irradiation by energetic ions commonly alters the surface and bulk properties of materials. Thus, ion irradiation can be used as a tool to tailor properties of materials with high relevance in, for example, thin-film electronics [1,2], surface nanostructure engineering and modification of 2D materials [3]. Irradiation of solid targets with either slow highly charged ions (HCI) [4–7] or swift heavy ions (SHI) [8–10] is widely studied and leads to nanoscale surface modification with potential applications in e.g., magnetic storage, nanoelectronics, catalysis and nanosensors [11,12]. HCI typically have velocities lower than the Bohr velocity ($v_B \approx 2.18 \times 10^6$ ms^{-1}) and potential energies due to vacant electron states on the order tens to hundreds of keV [13], while for SHI kinetic energies are on the order of tens of MeV to GeV. In the latter case, interaction with the target material is dominated by energy transfer to its electrons, characterized by the energy deposited on those electrons per unit path length, or electronic stopping power (S_e). Due to their larger bandgap, insulators are more sensitive than conductors or semiconductors to structural modifications induced by electronic excitations [14]. Irradiation of nonamorphizable insulators (crystalline materials with high ionicity and a low tendency for amorphization), e.g., fluorides (e.g., LiF, KBr, CaF_2, BaF_2) and some oxides (e.g., UO_2, SnO_2), results in various surface nanostructures such as pits, craters, calderas or nanohillocks [10–18].

A model system to study surface modification due to ion irradiation is Calcium Fluoride (CaF_2), a nonamorphizable ionic crystal with fluorite structure. It is widely investigated for the formation of nanoscale surface structures due to ion irradiation with HCI [19,20] and SHI [10,16]. In the case of HCI, the threshold for the formation of such nanostructures is defined in terms of potential energy while for SHI, the parameter of interest is S_e. Irradiation of CaF_2 with keV Xe ions yields nanoscale hillocks protruding from the surface for $q \geq 28+$, and etching the surface with 10 % HNO_3 solution leads to the formation of pyramidal pits. The threshold for such pit formation (after etching) depends on both potential energy and kinetic energy [19], whereas the threshold for nanohillocks formation by irradiation of CaF_2 surface with HCI depends dominantly on potential energy [20].

For irradiation of CaF_2 with SHI (^{48}Ca to ^{238}U) at specific energies from 1 to 11.1 MeV/u, the threshold S_e for nanoscale hillocks is reported to be ~4.8 ± 1.1 keV/nm [10]. Irradiation by SHI is also reported to produce near-surface modifications in CaF_2 with two thresholds in terms of S_e for damage creation [21]. These electronic energy loss threshold values depend on ion energy and correspond to (a) quenching of a molten phase, accompanied by swelling and surface nanohillock formation, and (b) quenching of a boiling phase leading to tracks visible in Transmission Electron Microscopy (TEM).

* Corresponding author.
E-mail address: rajdeep.kaur@physics.uu.se (R. Kaur).

https://doi.org/10.1016/j.nimb.2023.01.004
Received 25 July 2022; Received in revised form 10 November 2022; Accepted 6 January 2023
Available online 23 January 2023

Table 2.1
List of the projectiles used for irradiating CaF_2 samples with their kinetic energy (E_K), equilibrium charge state (q_{eq}), initial charge (q_{in}) and potential energy (E_P). * Irradiation with a fluence of 2×10^{10} ions/cm^2; ** 2.8×10^{10} ions/cm^2; # 5×10^{10} ions/cm^2; ## 1×10^{13} ions/cm^2 (if nothing else is specified, the fluence was 2×10^{11} ions/cm^2).

Ion	E_K (MeV)	q_{eq}	q_{in}	E_P (eV)	Ion	E_K (MeV)	q_{eq}	q_{in}	E_P (eV)
^{35}Cl	2.5	4.6	1+	13	^{79}Br	2.0##	4.5	1+	12
	3.5	5.3	2+	37		8.0	8.6	3+	68
	4.5	5.9	2+	37		8.5	8.8	3+	68
	7.0	6.9	3+	76		11.0	9.8	4+	116
	11.0	8.1	4+	130		13.5	10.7	5+	175
	15.0	8.9	5+	197		16.5	11.5	7+	366
	22.5*	10	7+	408		20.0	12.4	5+	175
	32.5	11	7+	408		40.0	15.7	9+	783
	40.0*	11.5	9+	1158	^{197}Au	3.0	5.2	2+	29
^{39}K	14#	9.2	6+	325		10.0	10.0	4+	104
^{52}Cr	12#	9.3	5+	173		17.0	13.0	5+	164
^{58}Ni	11	9.6	5+	192		21.5	14.5	7+	332
	25	12.8	8+	594		26.5	16.0	8+	130
	45	15.3	11+	1331		30.0	16.8	7+	444
						48.0**	20.5	11+	892

In the case of irradiation by highly charged medium energy ions (i.e., tens to hundreds of keV/u), the threshold for nanohillock formation can be defined by additive action of potential energy and S_e. For example, in irradiation with highly charged MeV Xe ions, the threshold charge for observing nanohillocks is between 25+ and 26+ with 3 MeV ($S_e = 0.72$ keV/nm) projectiles and between 21+ and 22+ with 5 MeV ($S_e = 1.46$ keV/nm) projectiles, indicating that the threshold for nanohillock formation in this energy regime depends on both kinetic energy and potential energy [22]. The threshold for the formation of these hillocks for MeV Xe ions is reported as $S_{et} \sim 2.75$ keV/nm, where S_{et} is the sum of weighted potential energy and S_e. This threshold value for medium energy ions is less than the S_e threshold reported for SHI [10,21] in the GeV regime approximately by a factor of 2.

In the present work, we investigate the surface structure modification in CaF_2 single crystals cleaved along the (1 1 1) plane in the lesser explored region of the lowly charged medium energy ions, where no effect of ion charge state in forming ion tracks is reported for CaF_2 [23]. All projectiles employed in this study, except for 32.5 MeV Cl and 40

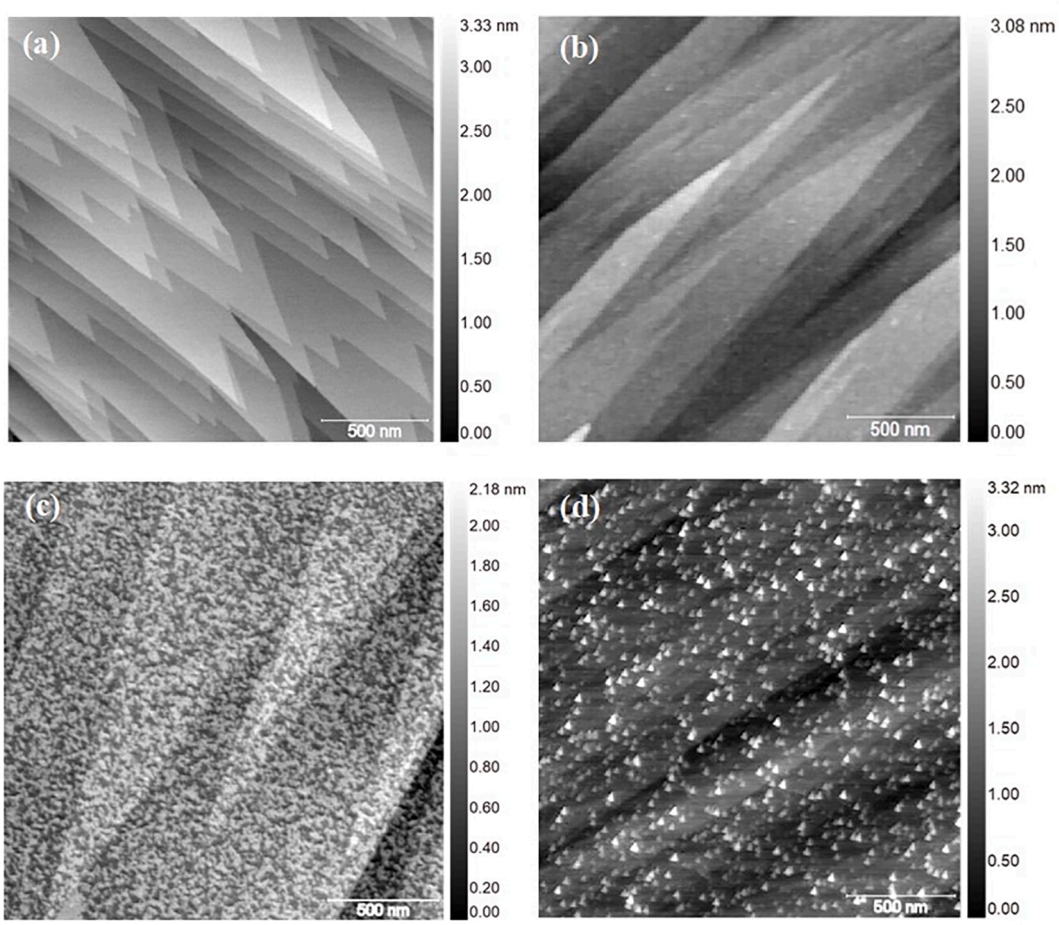

Fig. 3.1. AFM images for (a) unirradiated CaF_2 surface; surfaces irradiated with (b) 2 MeV Br^{1+}, (c) 7 MeV Cl^{3+} and (d) 30 MeV Au^{7+}. The fluence for all the irradiated surfaces was 2×10^{11} ions/cm^2.

MeV Cl, have energies below that for which S_e reaches its maximum value, as opposed to data reported with SHI where energies are above the same maximum. By bombarding CaF_2 with medium energy ions with a wide range of mass (*viz.*, ^{35}Cl, ^{39}K, ^{52}Cr, ^{58}Ni, ^{79}Br and ^{197}Au) and initial charge slightly below the equilibrium value eventually established as a result of electron exchange with the irradiated material, we investigate the threshold value for the formation of nanoscale surface structures in terms of projectile energy and S_e. In addition to the threshold values, the geometry of the nanostructures formed on the surface is analysed using atomic force microscopy (AFM).

2. Experimental

Single crystals of CaF_2 of (10×10) mm^2 square cross-section and a few mm height were produced by cleaving a larger crystal piece of CaF_2 along the (1 1 1) plane. The surface obtained from this cleavage features atomically flat terraces terminated by F-Ca-F triple layers. The minimum height between cleavage steps is 0.32 nm representing the height of one F-Ca-F triple layer [24]. The steps can be separated by an integral multiple of 0.32 nm. The naturally occurring steps on a CaF_2 (1 1 1) surface run essentially parallel to ⟨1 1 0⟩, ⟨2 1 1⟩ and ⟨3 2 1⟩ directions but are predominantly oriented along the ⟨1 1 0⟩ direction [25]. The cleaved crystals of CaF_2 were irradiated at room temperature under normal incidence by Cl, K, Cr, Ni, Br and Au ions with energies from 2 to 48 MeV. The equilibrium charge state for projectile ions was calculated using the formula for solid-state targets in the reference [26] and the initial charge state of the ions was kept below the equilibrium charge state, thus, ranging from 1+ to 11 +. To observe individual ion impact on the crystal surface, the ion fluences were kept low ranging from 2.0×10^{10} to 1×10^{13} ions/cm^2. The irradiation of samples was performed using a 5 MV pelletron tandem accelerator at Uppsala University [27].

Table 2.1 gives the complete list of the kinetic energy (E_K), equilibrium charge state (q_{eq}), initial charge (q_{in}) and potential energy (E_P) of the projectiles used to irradiate the CaF_2 samples. The potential energy of the charged particles was calculated using [28]. As observed from Table 2.1, the kinetic energy for each projectile ion is much higher ($>10^4$ times) than the potential energy for that ion. In addition to this, as the projectiles are further stripped to the equilibrium charge state upon entering the target material, rather than having their electronic states filled, the potential energy is not released near the surface. Thus, the potential energy is not expected to play an important role in producing damage on the CaF_2 surface in the present case. Most of the CaF_2 surfaces were irradiated with a fluence of 2×10^{11} ions/cm^2, with the exceptions mentioned in Table 2.1. Irradiations with lower fluence were performed to distinctly see the shape of nanostructures produced by a single ion impact.

The surface properties of the irradiated samples were studied by the means of Atomic Force Microscopy (AFM) in contact mode using PSIA XE150 AFM. AFM image processing was performed using the Gwyddion software [29]. Stopping powers for the projectiles of the given energy were calculated using SRIM [30]. These values were used to study the dependence of surface structure modifications in single crystals on stopping power.

3. Results

Depending on the energy of the projectile ion, different surface morphologies have been observed on the irradiated surfaces as shown in Fig. 3.1. Fig. 3.1(a) shows an AFM image obtained on the unirradiated CaF_2 surface; the remaining subfigures show surfaces irradiated with (b) 2 MeV Br^{1+}, (c) 7 MeV Cl^{3+} and (d) 30 MeV Au^{7+}. In Fig. 3.1(a), the surface morphology is dominated by flat cleaving terraces with a step height of 0.32 nm or an integer multiple of 0.32 nm and, enclosing angles of (11°–12°), (19°–22°) and (30°–34°). The angle of 11° corresponds to the apex angle between [2 1 1] and [3 2 1], 19° corresponds to the apex angle between [1 1 0] and [3 2 1] and 30° corresponds to the apex angle between [1 1 0] and [2 1 1]. Deviation from the exact apex angles between crystallographic directions may be caused due to lateral resolution of AFM images. In Fig. 3.2(b), the overall structure of the surface is still dominated by terraces caused by cleavage of CaF_2 along the (1 1 1) plane. Clear modification of the surface dominated by irregular structures of vertical variation of less than 2 nm is seen in Fig. 3.1 (c), whereas, distinct triangular structures of height less than 3.5 nm are observed in Fig. 3.1(d).

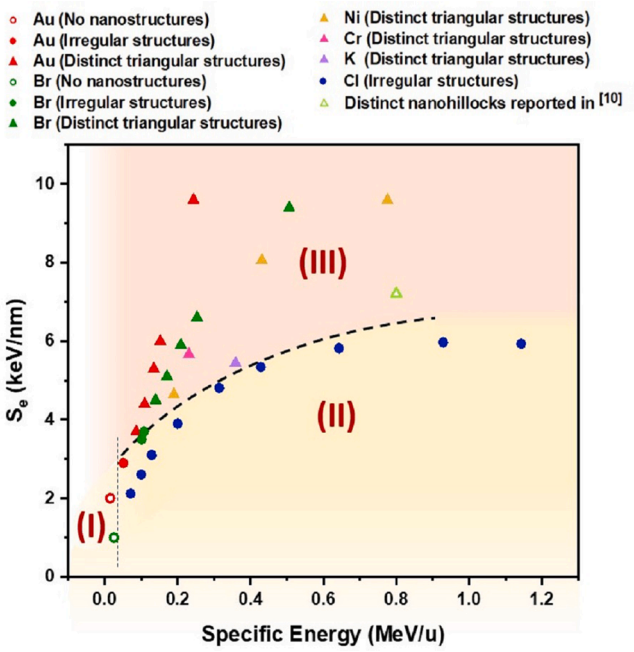

Fig. 3.2. Region (I): hollow circles indicate pairs of specific energy and S_e for which minimum modification is observed (as seen in Fig. 3.1(b)); **Region (II):** solid circles indicate pairs for which irregular structures are observed (as seen in Fig. 3.1(c)) and; **Region (III):** triangles indicate pairs for which distinct triangular structures are observed (as seen in Fig. 3.1(d)). Projectile ions of different elements are indicated by different colours as mentioned in the legend.

Based on the different surface morphologies observed on the ion-irradiated CaF_2 surfaces, a threshold for surface modification in terms of specific energy and S_e is found. Fig. 3.2 places all projectiles employed in this study on a map of specific energy and S_e. Three different regions have been identified: region (I) with minimum modification of the surface, region (II) with irregular structures and region (III) with distinct triangular structures of height between 0.5 and 6 nm (for the ions employed in this work). Two cases with irradiating ions below a specific energy of approximately 0.04 MeV/u and S_e below 2 keV/nm caused no or only slight modification of the surface. For the remaining projectiles, a threshold in electronic stopping power, S_{et}, is required to form distinct triangular structures on the surface. Below S_{et}, irregular structures are observed on the surface. There is no sudden transition from irregular structures to distinct structures, but a gradual increase in the dominance of distinct triangular structures over the irregular structures as the energy of ions increases. S_{et} is defined as the point where distinct triangular structures start becoming clearly visible on the surface. The value of S_{et} increases with the energy of the projectile ions. For instance: for ions with energy of ~0.08 MeV/u, distinct triangular structures on the surface are observed for $S_e \sim 3.7$ keV/nm (17 MeV Au). But for irradiation with ions of similar $S_e \sim 3.9$ keV/nm (7 MeV Cl) at a higher energy of ~0.2 MeV/u, irregular structures are observed. Distinct triangular structures for ions with energy of ~0.2 MeV/u are observed for $S_e \sim 4.7$ keV/nm (11 MeV Ni).

The irregular structures dominating the surface in the region (II) have a vertical variation of <2 nm. The distinct triangular structures observed in the region (III) are not of the same height but have a range of

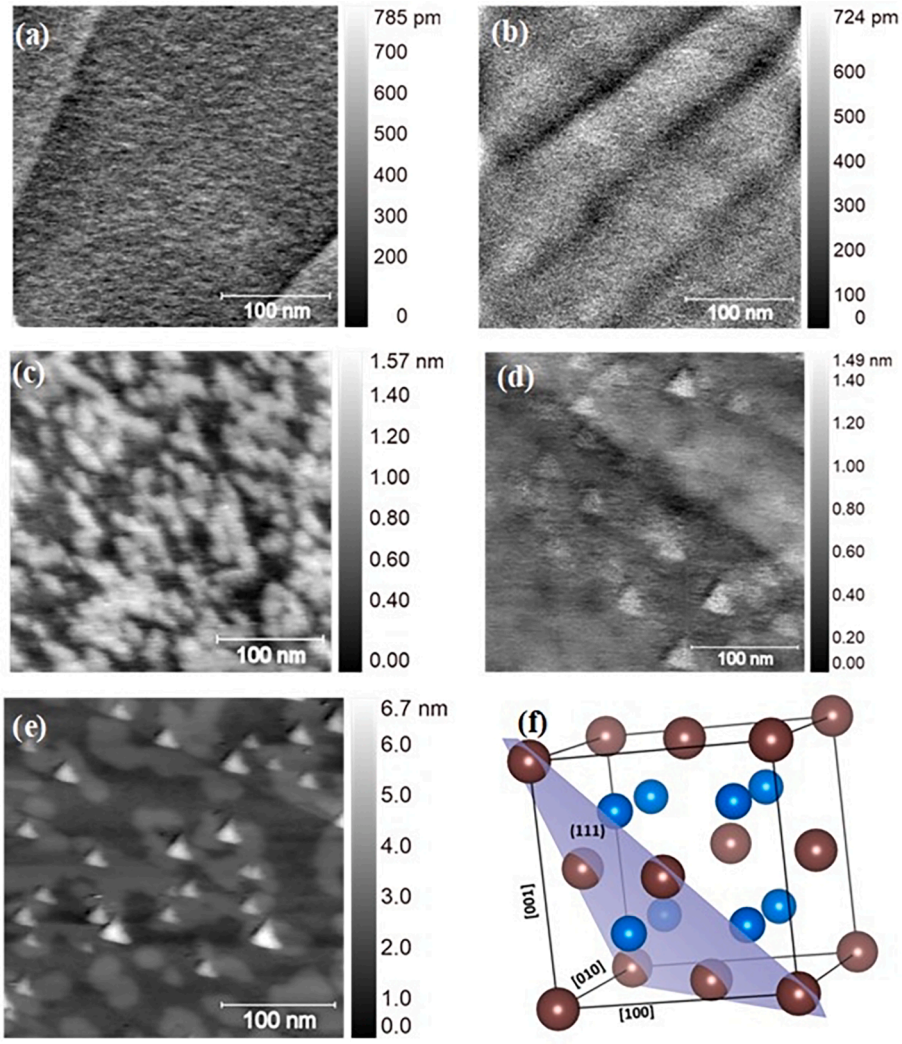

Fig. 3.3. AFM images for (a) unirradiated surface; and surfaces irradiated by (b) 2 MeV Br^{1+} [fluence = 2×10^{11} ions/cm^2], (c) 7 MeV Cl^{3+} [fluence = 2×10^{11} ions/cm^2], (d) 17 MeV Au^{5+} [fluence = 2×10^{11} ions/cm^2] and (e) 48 MeV Au^{11+} [fluence = 2.8×10^{10} ions/cm^2]; (f) Schematic of a unit cell of CaF_2 along with (1 1 1) plane cutting through the unit cell [drawn using VESTA [31]].

height, e.g., for irradiation with 48 MeV Au, the observed height of nanostructures range from 2 to 6 nm. Magnified images of the unirradiated surface as well as a selection of irradiated surfaces are shown in Fig. 3.3. Nanostructures protruding from the surface have approximately equilateral triangular bases (within the limit of the lateral resolution of AFM images). One possible orientation of these equilateral

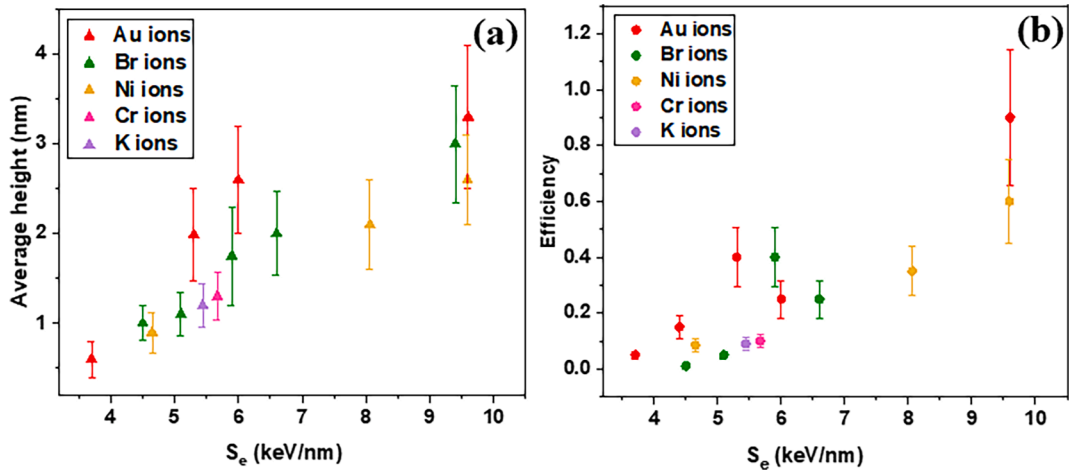

Fig. 3.4. (a) The average height of triangular nanostructures as a function of S_e and (b) Mean efficiency of formation for triangular nanostructures as a function of S_e.

triangular bases, as seen in Fig. 3.3(f), can be that the limiting surfaces of the protruding structures are aligned with {1 0 0} planes of the original crystal. However, in the present data, the height-to-width ratio of the nanostructures is not consistent with triangular structures in the form of perfect pyramids, recrystallized to complete the unit cell above the (1 1 1) plane. In order to substantiate or discard any such claim about the lattice orientation of the protrusions, a more detailed investigation into the accuracy of the absolute height measurement of the AFM when scanning over both radiation-damaged and undamaged material would therefore have to be carried out.

The height (h) is determined by extracting profiles along different lines and calculating the maximum deviation in the vertical direction from the surrounding plane. The height of almost all the clearly visible non-overlapping triangular structures was calculated for 2 to 5 separate AFM images taken over different regions of the surface to plot the variation of average height with S_e. For example: in the case of the sample irradiated with 48 MeV Au^{11+}, three AFM images with 28 [scan area: (500 × 500) nm^2], 23 [scan area: (300 × 300) nm^2] and 16 [scan area: (200 × 200) nm^2] structures were studied. Fig. 3.4(a) shows the average height of nanostructures formed on the surface as a function of S_e, where the standard deviation of the height distribution for each ion is given as an error in the average height. The average height of the triangular structures in the region (III) increases with stopping power.

The efficiency of nanostructure formation is defined as the ratio of the number of distinct nanostructures observed on the surface to the number of incident ions. An efficiency of 1 implies that each incident ion produced a nanostructure on the surface. While counting the number of nanostructures from AFM images, some partly overlapping structures are also observed. These partly overlapping structures are assumed to be the resultant of different single ion impacts and are counted separately. The number of incident ions can be calculated from the values of the initial charge, ion current, area of irradiation and time for irradiation. Fig. 3.4(b) shows the average efficiency of nanostructures formed on the surface as a function of S_e. The observed efficiency for the formation of nanostructures is not 1 for all irradiations. Instead, the efficiency of nanostructure formation in the region (III) increases with S_e for medium energy ions. We have assumed an uncertainty of 25 % on the scan area and a 10 % uncertainty on the ion current and thus, as observed from Fig. 3.4(b), the change in formation efficiency is not estimated to be an artefact of the measurements of ion current and scan area.

4. Conclusions and discussion

Surface modification of single crystalline CaF_2 by irradiation with MeV energy ions was studied using Atomic Force Microscopy. From the study of AFM images of the irradiated surfaces, we infer that projectile ions with specific energy above approximately 0.04 MeV/u cause clearly detectable modification on the surface of the crystal. A threshold in terms of S_e distinguishes between two types of surface modification. Below the threshold value, the modified surface is dominated by irregular structures of vertical variation less than 2 nm, and above S_{et}, the surface is dominated by distinct triangular nanostructures of height from 0.5 to 6 nm produced by a single ion impact. The triangular structures have apparently equilateral triangular bases.

Unlike in the case of SHI [10] where the average height of hillocks is constant (~1 nm) for S_e between 5 and 10 keV/nm, the average height of the distinct triangular structures increases from ~0.5 nm to ~3.3 nm for irradiation by medium energy ions in this range of S_e. The efficiency of nanostructure formation increases with S_e, which is in agreement with the results observed for irradiation by SHI [10,21].

As indicated by the dashed curve in Fig. 3.2, the value of S_{et} increases non-linearly with the energy of the projectile ions. Both the value of S_{et} and its energy scaling are consistent with the previously reported results on the threshold for local melting [21,22]. The increase in S_{et} with specific energy and, thus with ion velocity, can be attributed to the well-known 'velocity effect' [22], referring to the influence of the velocity of projectiles on the damage caused by the ion irradiation.

The initial charge state of projectiles in the present study is below the equilibrium charge state, approximately by a factor of (0.4–0.6); thus, the initial value of S_e is ~ (0.16–0.25) times the equilibrium S_e (plotted here). As the ion traverses the target, it gains charge to reach the equilibrium charge state and consequently, the value of S_e increases as the projectile traverses the target. The equilibration length, (d) [32], is of the order of a few nanometres, comparable to the height of triangular nanostructures observed in the region (III) (for example: d ~ 5 nm for 30 MeV Au). A follow-up experiment can be performed for the projectiles in the region (III), e.g., irradiation with 13.5 MeV Br (equilibrium charge ~10.7 ± 1.5) [26] with charge states from 3+ to 11+, to study how height and formation efficiency of nanostructures are affected by the difference in the initial and the equilibrium charge state. Data on the charge state independence of ion track widths in CaF_2 irradiated by ^{127}I in [23] supports the hypothesis that charge state equilibration might not have a critical effect on the stopping power thresholds reported in the present work.

Declaration of Competing Interest

The authors declare that they have no known competing financial interests or personal relationships that could have appeared to influence the work reported in this paper.

Acknowledgements

We acknowledge financial support from the Swedish Research Council, VR-RFI (contract #2019-00191) and the Swedish Foundation for Strategic Research (SSF, contract RIF14-0053) supporting the accelerator operation. We are grateful to Amit Patel, Research Engineer at MyFab Uppsala, for technical support and assistance with initial AFM measurements.

References

[1] X. Xiang, Z. He, J. Rao, Z. Fan, X. Wang, Y. Chen, Applications of ion beam irradiation in multifunctional oxide thin films: A review, ACS Appl. Electron. Mater. 3 (3) (2021) 1031–1042.
[2] R. Panda, S.A. Khan, U.P. Singh, R. Naik, N.C. Mishra, The impact of fluence dependent 120 MeV Ag swift heavy ion irradiation on the changes in structural, electronic, and optical properties of $AgInSe_2$ nano-crystalline thin films for optoelectronic applications, RSC Adv. 11 (42) (2021) 26218–26227.
[3] Z. Li, F. Chen, Ion beam modification of two-dimensional materials: Characterization, properties, and applications, Appl. Phys. Rev. 4 (1) (2017), 011103.
[4] T. Peters, C. Haake, J. Hopster, V. Sokolovsky, A. Wucher, M. Schleberger, HICS: Highly charged ion collisions with surfaces, Nucl. Instrum. Methods Phys. Res. Sect. B Beam Interact. Mater. At. 267 (4) (2009) 687–690.
[5] R. Ritter, R.A. Wilhelm, R. Ginzel, G. Kowarik, R. Heller, A.S. El-Said, R. M. Papaléo, W. Rupp, J.R. Crespo López-Urrutia, J. Ullrich, S. Facsko, F. Aumayr, Pit formation on poly (methyl methacrylate) due to ablation induced by individual slow highly charged ion impact, EPL Europhys Lett. 97 (1) (2012) 13001.
[6] M. Tona, Y. Fujita, C. Yamada, S. Ohtani, Electronic interaction of individual slow highly charged ions with TiO_2 (110), Phys. Rev. B 77 (15) (2008), 155427.
[7] P. Li, H. Zhang, L. Wei, B. Niu, H. Yuan, Z. Cheng, H. Zhang, Z. Yang, Y. Guo, Y. Ma, C. Wan, Y. Cui, M. Li, X. Chen, Surface nanostructures formation induced by highly charged ions: Kinetic and potential energy dependence, Nucl. Instrum. Methods Phys. Res. Sect. B Beam Interact. Mater. At. 513 (2022) 14–20.
[8] N. Ishikawa, T. Taguchi, N. Okubo, Hillocks created for amorphizable and non-amorphizable ceramics irradiated with swift heavy ions: TEM study, Nanotechnology 28 (44) (2017), 445708.
[9] N. Khalfaoui, C.C. Rotaru, S. Bouffard, E. Jacquet, H. Lebius, M. Toulemonde, Study of swift heavy ion tracks on crystalline quartz surfaces, Nucl. Instrum. Methods Phys. Res. Sect. B Beam Interact. Mater. At. 209 (2003) 165–169.
[10] N. Khalfaoui, C.C. Rotaru, S. Bouffard, M. Toulemonde, J.P. Stoquert, F. Haas, C. Trautmann, J. Jensen, A. Dunlop, Characterization of swift heavy ion tracks in CaF_2 by scanning force and transmission electron microscopy, Nucl. Instrum. Methods Phys. Res. Sect. B Beam Interact. Mater. At. 240 (4) (2005) 819–828.
[11] W. Li, X. Zhan, X. Song, S. Si, R. Chen, J. Liu, Z. Wang, J. He, X. Xiao, A Review of recent applications of ion beam techniques on nanomaterial surface modification: design of nanostructures and energy harvesting, Small 15 (31) (2019) 1901820.
[12] J. Muñoz-García, L. Vázquez, R. Cuerno, J.A. Sánchez-García, M. Castro, R. Gago, Self-organized surface nanopatterning by ion beam sputtering, in: Z.M. Wang (Ed.) Toward Functional Nanomaterials [Internet]. New York, NY: Springer US; 2009

[cited 2022 Jul 4]. pp. 323–398. Available from: http://link.springer.com/10.1007/978-0-387-77717-7_10.
[13] F. Aumayr, S. Facsko, A.S. El-Said, C. Trautmann, M. Schleberger, Single ion-induced surface nanostructures a comparison between slow highly-charged and swift heavy ions, J. Phys.: Condens. Matter. 23 (39) (2011), 393001.
[14] A.S. El-Said, R. Heller, R.A. Wilhelm, S. Facsko, F. Aumayr, Surface modifications of BaF_2 and CaF_2 single crystals by slow highly charged ions, Appl. Surf. Sci. 310 (2014) 169–173.
[15] R. Heller, S. Facsko, R.A. Wilhelm, W. Möller, Defect mediated desorption of the KBr (001) surface induced by single highly charged ion impact, Phys. Rev. Lett. 101 (9) (2008), 096102.
[16] C. Müller, M. Cranney, A. El-Said, N. Ishikawa, A. Iwase, M. Lang, R. Neumann, Ion tracks on LiF and CaF_2 single crystals characterized by scanning force microscopy, Nucl. Instrum. Methods Phys. Res. Sect. B Beam Interact. Mater. At. 191 (1-4) (2002) 246–250.
[17] A.S. El-Said, R.A. Wilhelm, R. Heller, M. Sorokin, S. Facsko, F. Aumayr, Tuning the fabrication of nanostructures by low-energy highly charged ions, Phys. Rev. Lett. 117 (12) (2016), 126101.
[18] A. Müller, C. Müller, R. Neumann, F. Ohnesorge, Scanning force microscopy of heavy-ion induced damage in lithium fluoride single-crystals, Nucl. Instrum. Methods Phys. Res. Sect. B Beam Interact. Mater. At. 166–167 (2000) 581–585.
[19] A.S. El-Said, R.A. Wilhelm, R. Heller, S. Facsko, C. Lemell, G. Wachter, et al., Phase diagram for nanostructuring CaF_2 surfaces by slow highly charged ions, Phys. Rev. Lett. 109 (11) (2012), 117602.
[20] A.S. El-Said, R.A. Wilhelm, R. Heller, R. Ritter, G. Wachter, S. Facsko, C. Lemell, J. Burgdörfer, F. Aumayr, Nanostructuring CaF_2 surfaces with slow highly charged ions, J. Phys. Conf. Ser. 488 (1) (2014), 012002.
[21] M. Toulemonde, A. Benyagoub, C. Trautmann, N. Khalfaoui, M. Boccanfuso, C. Dufour, et al., Dense and nanometric electronic excitations induced by swift heavy ions in an ionic CaF_2 crystal: Evidence for two thresholds of damage creation, Phys. Rev. B 85 (5) (2012), 054112.
[22] Y.Y. Wang, C. Grygiel, C. Dufour, J.R. Sun, Z.G. Wang, Y.T. Zhao, G.Q. Xiao, R. Cheng, X.M. Zhou, J.R. Ren, S.D. Liu, Y. Lei, Y.B. Sun, R. Ritter, E. Gruber, A. Cassimi, I. Monnet, S. Bouffard, F. Aumayr, M. Toulemonde, Energy deposition by heavy ions: additivity of kinetic and potential energy contributions in hillock formation on CaF_2, Sci. Rep. 4 (1) (2015) 5742.
[23] K. Tomić Luketić, J. Hanžek, C.G. Mihalcea, P. Dubček, A. Gajović, Z. Siketić, M. Jakšić, C. Ghica, M. Karlušić, Charge state effects in swift-heavy-ion-irradiated nanomaterials, Crystals 12 (6) (2022) 865.
[24] J.B. Engelhardt, H. Dabringhaus, K. Wandelt, Atomic force microscopy study of the CaF_2(111) surface: from cleavage via island to evaporation topographies, Surf. Sci. 448 (2–3) (2000) 187–200.
[25] C. Motzer, M. Reichling, High resolution study of etch figures on CaF_2 (111), J. Appl. Phys. 105 (6) (2009), 064309.
[26] G. Schiwietz, P.L. Grande, Improved charge-state formulas, Nucl. Instrum. Methods Phys. Res. Sect. B Beam Interact. Mater. At. 175–177 (2001) 125–131.
[27] P. Ström, D. Primetzhofer, Ion beam tools for nondestructive in-situ and in-operando composition analysis and modification of materials at the Tandem Laboratory in Uppsala, J. Instrum. 17 (04) (2022) P04011.
[28] A. Kramida, Y. Ralchenko, NIST Atomic Spectra Database, NIST Standard Reference Database 78 [Online]. National Institute of Standards and Technology; 1999 [cited 2022 May 15]. Available from: http://www.nist.gov/pml/data/asd.cfm. (Date of Access: 2022-06-01).
[29] D. Nečas, P. Klapetek, Gwyddion: an open-source software for SPM data analysis. Cent. Eur. J. Phys. 10(1) (2012) 181-188, Available from: http://gwyddion.net/. (Date of Access: 2022-07-01).
[30] J.F. Ziegler, M.D. Ziegler, J.P. Biersack, SRIM – The stopping and range of ions in matter (2010), Nucl. Instrum. Methods Phys. Res. Sect. B Beam Interact. Mater. At. 268 (11–12) (2010) 1818–1823.
[31] K. Momma, F. Izumi, VESTA 3 for three-dimensional visualization of crystal, volumetric and morphology data, Available from, J. Appl. Cryst. 44 (2011) 1272–1276, https://jp-minerals.org/en/.
[32] P. Ström, D. Primetzhofer, Energy deposition by nonequilibrium charge states of MeV ^{127}I in Au, Phys. Rev. A 103 (2) (2021), 022803.